Facile and Rapid Fabrication of Opal Photonic Crystals by Electrophoretic Deposition

Clement Lebastard[1,2]*†, *Yousra Hattali*[1,2,3], *Antoine Le Gendre*[3], *Stephane Cordier,*[3] *Adèle Renaud*[3], *Tohru Suzuki*[1,2], *Tetsuo Uchikoshi*[1,2*], *Fabien Grasset*[1,2]

[1]CNRS-Saint Gobain-NIMS, IRL 3629, Laboratory for Innovative Key Materials and Structures (LINK), National Institute for Materials Science (NIMS), Tsukuba, 305-0044, Japan

[2]National Institute for Materials Science (NIMS), 1-2-1 Sengen, Tsukuba, Ibaraki 305-0047, Japan

[3]Université de Rennes, CNRS, UMR6226, Institut des Sciences Chimiques de Rennes (ISCR), F-35000 Rennes, France

*Corresponding authors: clement.lebastard@ensc-rennes.fr, uchikoshi.tetsuo@nims.go.jp

†Université de Rennes, Ecole Nationale Supérieure de Chimie de Rennes

CNRS, UMR6226, Institut des Sciences Chimiques de Rennes (ISCR), F-35000 Rennes, France

KEYWORDS

Electrophoretic deposition, SiO_2, photonic crystal, opal structure, self-assembly

ABSTRACT

The use of photonic crystals (PCs) is gaining in interest regarding the interaction between light and organized structures. However, there are limitations to their use, including production cost, rate and substrate size. This study demonstrates an efficient and cost-effective fabrication of an opal structure based on the electrophoretic deposition (EPD) of self-made silica particles. The process allows to reduce the fabrication time compared to classical evaporation or sedimentation methods, which can take days (evaporation) or weeks to months (sedimentation), while this method takes only two minutes. Silica particles with a diameter of less than 300 nm exhibit a markedly low sedimentation rate. Nevertheless, when they form a close-packed structure, they display a partial band gap in the visible region. The resulting opals are iridescent, from blue to red, and display additional angle-dependent colors. Furthermore, the synthesis of silica particles was completed within a two-hour timeframe. Their washing, including a centrifugation step, did not result in the formation of aggregates. Such particles tend to break the long-range order in the PCs.

INTRODUCTION

In the contemporary age of miniaturization, photonic crystals (PCs) are emerging as significant structures for guiding and manipulating light, as well as for information transfer and processing in a multitude of optical,[1,2] multifunctional,[3] or sensing applications.[4] First observed in nature, PCs give the iridescent colors of butterfly wings, beetle shells or opal gemstones.[5] Colors do not originate from a natural pigmentation or a certain wavelength absorption; rather, they result from the interaction of light with the periodic structure of the PCs. Researchers are attempting to reproduce these structures through top-down and bottom-up approaches. While the first method often necessitates the use of costly and sophisticated equipment, such as lithographic apparatus

and clean room facilities, the second method is typically favored. The formation of PCs is typically achieved through the self-assembly of colloidal particles, which can occur through a number of methods, including natural sedimentation,[6,7] solvent evaporation,[8] or Langmuir-Blodgett technique[9] which employs the use of polystyrene microspheres or silica particles. The formation rate of PCs is faster with a bottom-up approach but it is susceptible to lack of control compared to a top-down approach. Furthermore, it may still be too slow for industrial production. The majority of the current self-assembly techniques require several hours or days to complete.[10–12] However, there are alternative methods that have been less widely explored but which can achieve a faster self-assembly on a large scale. EPD is a promising method to form PCs in a relatively short time frame and on a range of substrate geometries.[13] This process, which has already been employed in the coating industry, this process relies on electrophoresis, *i.e.* the migration of charged particles in a solution under the application of an electric field, and on the use of a conductive substrate where the particles will settle and coagulate. This process allows for the rapid coating of porous materials and complex shapes, making it a versatile, low-energy and cost-effective option for a range of applications.[14,15] In 1997, Mayoral *et al*.[6] identified a 3D long-range ordered compact structure of silica particles through the sedimentation process. Subsequently, in 1999,[16] they published the initial combination of sedimentation and electrophoretic processes. In general, silica particles outside of the 300 – 550 nm size range are not suitable for a sedimentation method. On the one hand, the gravitational force can be compensated for by thermal agitation if the SiO_2 particles are smaller than 300 nm. On the other hand, when SiO_2 particles exceed 550 nm in size, the gravitational force surpasses the thermal agitation, resulting in a deviation from equilibrium and the formation of a non-iridescent photonic glass. In their study,[16] an electric field was employed to increase the velocity of small particles (under 300 nm) with the objective of reducing

the time required for PCs to form. In contrast, the sedimentation of particles larger than 550 nm was retarded by applying an electric field in opposition to gravity. In 2000, Rogach *et al*.[17] achieved the production of polystyrene (PS) 3D PCs by EPD, with the same quality as that obtained through the sedimentation process. Notably, the formation time was reduced from weeks or months to just 30 minutes. Since that date, a number of advances have emerged including improvements in quality, faster deposition times, larger substrate sizes and a broader range of particle sizes. Recently, Tran *et al*.[18] investigated the optimal condition for forming PS PCs, while Katagiri *et al*.[19] reported a 25-minute EPD with SiO_2 particles. In this final study, the researchers observed the formation of an amorphous array of colloidal particles when the voltage exceeded 60 V. When the particle velocity was too high, the rearrangement of the particles could not be optimized, resulting in an amorphous array that lacked periodicity. This phenomenon was also observed in the spray-coating method.[20] The use of a high voltage can also generate gas through the electrolysis of water.[21]

In this paper, we synthesized SiO_2 particles with diameters ranging from approximately 180 to 310 nm. It roughly corresponds to the diameter of monodisperse spheres that can be found in natural non-crystalline opal (150 – 350 nm).[22] Additionally, this diameter range falls within the range where sedimentation can be significantly prolonged or occur concurrently with thermal agitation. The fabrication of 3D PCs on vertical indium-tin oxide (ITO) glass substrate through EPD was investigated with respect to the applied voltage and duration, as well as the choice of dispersion solvent and particle size. It was demonstrated that PCs exhibiting a photonic band gap (PBG) could be produced across the entire visible spectrum (≈ 390-660 nm).

EXPERIMENTAL SECTION

Chemicals. Ethanol (99.5%; Wako), ammonia solution (noted NH_3, 28 wt. %; Wako), ultra-purified water (noted H_2O, KYK), tetraethyl orthosilicate (noted TEOS, 99%; Sigma-Aldrich) and 1-propanol (99.5%, Nacalai tesque) were used as starting precursors and/or solvent. No extra steps of purification were achieved. Indium doped tin oxide (noted ITO) glass (10 Ω/sq) (Geomatec Co., Ltd., Japan) was used as the conductive substrate.

Synthesis. The SiO_2 nanoparticles were synthetized following the Stöber method,[23] where silicone alkoxide is first hydrolyzed before undergoing a condensation step, catalyzed by the basic environment of the suspension (Figure S1). In our case, 4.5 mL of water and 12 mL of ammonia were added to a large volume of ethanol ranging from 40 to 75 mL. After homogenization at 60 °C, 9 mL of TEOS were added in the round bottom flask and left for 2 hours. Initially transparent, the suspension became opalescent at first before becoming totally white and opaque after a few minutes only. The required time to reach the opalescent step and then the opaque one relies on the volume of ethanol used. However, it became opaque in less than 5 minutes for every solution. The suspensions were then left to cool down for 30 minutes, and transferred to centrifuge tubes. Silica nanoparticles were collected after 15 min at 10 000 RPM by using an AS185 centrifuge (AS ONE) equipped with a 6 × 50 mL rotor (radius 9.5 cm). Particles were then redispersed in 20 mL of ethanol and centrifuged again. In order to remove impurities, three cycles were carried out. Dried nanoparticles were recovered prior their redispersion in alcohols or alcohols-water mixtures for EPD (1 wt%). Methanol was avoided because of its toxicity but ethanol and 1-propanol were used as pure solvent or with water (volume ratio 4:1).

EPD. Electrophoretic deposition was performed with a large volume to avoid a drastic diminution in the concentration over the preparation of numerous samples. Typically, 237 mg of nanoparticles were redispersed in 30 mL of ethanol, combining strong stirring and sonication for one hour. ITO glass was used as electrodes (both anode and cathode) and prepared by cutting 2.5 × 1 cm rectangles or 2.5 × 2.5 cm squares. They were cleaned in three successive sonicated baths for 30 min (deionized water, ethanol and acetone). Electrodes were vertically placed facing each other, separated by a 5 mm gap, immersed in a beaker containing the colloidal solution and connected to an electric field generator (Anatech Model 3870 (Anatech, Japan)) thanks to metallic bar and carbon tape. Depositions were done at a voltage ranging from 10 to 25 V for 30 seconds to 5 minutes. Films were recovered at a withdrawing speed of 12 mm/sec (Auto lab jack (As One, Japan)) and left to dry at room temperature (20°C – 40-50% humidity). Figure 1 shows the different steps from the SiO_2 synthesis by the Stöber method to the formation of PCs through EPD.

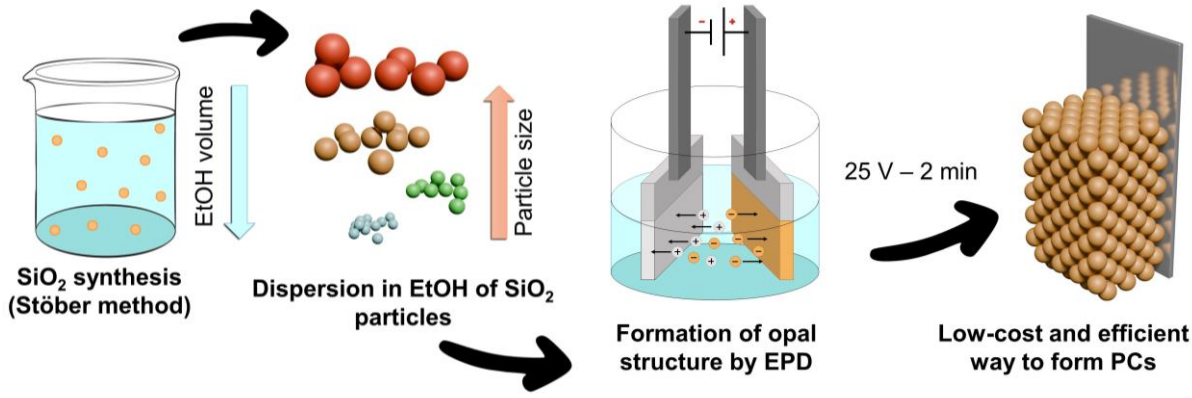

Figure 1. Schematic diagram of the SiO_2 synthesis to the EPD process.

Sedimentation. Sedimentation rates were evaluated in closed container at room temperature, with a humidity ranging from 40 to 50 % (in the room). Containers were disposed on an isolated surface to prevent the vibrations (Figure S2). A standard was placed next to the containers and

pictures were taken at different time. Measurement of the suspension and the whole volume (solvent + suspension beneath) was done with the image processing and analysis software ImageJ.

Characterizations. The dynamic light scattering (DLS) and Zeta potential measurements were taken using diluted dispersion of nanoparticles in alcohol or alcohol-water mixtures (0.5 $mg \cdot mL^{-1}$). A cumulant method was used to fit the correlation function. An ELSZ-2000ZS (Otsuka Electronics Co. Ltd., Japan) and a Malvern Zetasizer Nano Z (Malvern Instruments Ltd., U.K.) were respectively used. Thin films were characterized by X-ray diffraction using a Rigaku Smart Lab (Rigaku, Japan). Measurements were done from 10 to 80°, with a 0.02° step width, a scan speed of $5° \cdot min^{-1}$ and with a Cu Kα radiation. UV−vis transmittance and reflectance measurements were taken using a V-770 UV−vis-NIR spectrophotometer (JASCO Co., Japan). SEM pictures were obtained with a S-4800 FE SEM (Hitachi, Japan) with an accelerating voltage of 10 kV.

RESULTS AND DISCUSSION

Since the publication of Stöber's *et al*.[23] paper on the synthesis of monodisperse silica spheres (see Supporting Information & Figure S1), numerous studies have highlighted the influence of precursors concentration, temperature, pH and total volume on the particle size and polydispersity.[24,25] In our study we decided to only vary the volume of ethanol while keeping the other parameters fixed (temperature, volumes of other precursors).[26,27] The amount of H_2O/NH_3/TEOS was fixed to 4.5/12/9 mL for a varying volume of ethanol from 40 to 75 mL (syntheses are noted from SiO_2-40 to SiO_2-75 respectively). The temperature of the reaction was fixed at 60 °C. The particle size was subsequently determined by DLS following the washing and redispersion steps (in pure ethanol), with a range of 178 to 309 nm. Table 1 presents a compilation

of the synthesis parameters and the corresponding DLS results, which illustrate a reduction in nanoparticle size with an increase in the initial ethanol volume.

Table 1. SiO_2 particles synthesis parameter and diameter evaluations.

		DLS		SEM		UV-Vis	
V_{EtOH} (mL)	[TEOS] ($mol.L^{-1}$)	d_{DLS} (nm)	PDI	d_{SEM} (nm)	σ	λ_{refl} (nm)	d_{calc} (nm)
75	0.40	178	0.027	169	8	391	181
65	0.44	230	0.052	226	12	515	239
60	0.47	259	0.011	251	11	577	267
50	0.52	284	0.035	277	15	626	290
45	0.57	302	0.054	287	12	648	300
40	0.61	309	0.044	302	13	661	306

As previously stated in the experimental section, the washed nanoparticles were redispersed in two distinct types of alcohol and water-alcohol mixtures (1 wt%) through a combination of sonication and stirring. This approach was employed to prevent the formation of small aggregates during the deposition process. The sedimentation of nanoparticles is fundamentally slow enough to proceed to EPD without the impact of the gravity in that short deposition time. Sedimentation rates were evaluated over a long period of time in ethanol and compared to the Stokes law model (Equation 1). With *v* the velocity, D the diameter of the silica particles, ρ_{SiO_2} the density of silica, ρ_{EtOH} the density of ethanol, g the gravity and η the viscosity of ethanol.[6]

$$v = \frac{D^2 \cdot (\rho_{SiO_2} - \rho_{EtOH}) \cdot g}{18 \cdot \eta} \qquad \text{(Equation 1)}$$

For each measurement, the ratio between the height of the sedimentation was compared to the height of the entire volume. As anticipated, larger nanoparticles fall down faster than smaller one, *i.e.* ≈ 200 hours for SiO_2-40 and ≈ 900 hours for SiO_2-75. However, for each synthesis, the silica

particles exhibit a polydisperse distribution (0.01 < PDI < 0.05) which imply some disparity in the sedimentation rate. The highest part of the sedimentation volume contains smaller particles whereas the bottom part of the volume contains larger particles. Because the evaluation of sedimentation rates is done by measuring the top of the sedimentation height, its value is biased regarding the average size of the batch. Indeed, we observed a shift between the particles size measured by DLS and the one calculated by the Stokes law, with the experimental sedimentation rate time. For the sake of comparison, theoretical sedimentation rates were evaluated thanks to the Stokes law, based on SiO_2 particles size measured by DLS. The theoretical times required for a full sedimentation are gathered in Table 2 and the sedimentation rates of 2 samples are represented in Figure 2 (the whole series is in the Supporting Information, Figure S3). Despite the experimental-theoretical sedimentation rate gap, the time required for a full sedimentation is coherent with a single sphere sedimentation, no aggregates are formed. Overall, the time required for a complete sedimentation (hundreds of hours) is clearly not in the same magnitude order of the time required for the EPD (few minutes).

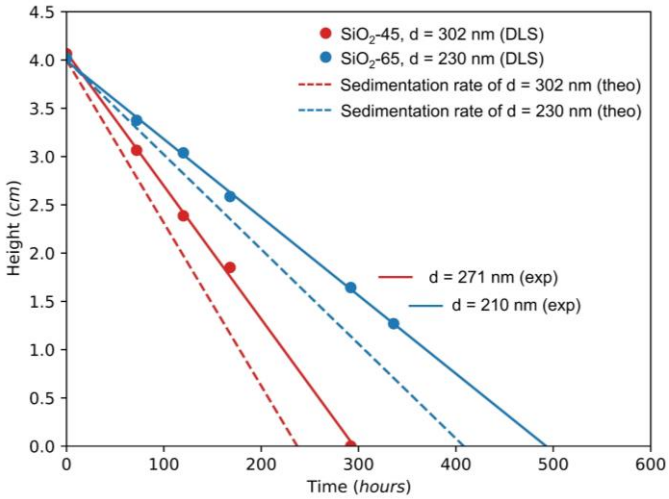

Figure 2. Sedimentation rate of SiO_2-45 (red) and SiO_2-65 (blue) as a function of time. Solid lines represent the sedimentation rates based on the measured height of sedimentation (dots) and dashed lines represents the theoretical rates based on DLS particles size.

Table 2. Sedimentation time and SiO_2 particles size based on Stokes's law.

V_{EtOH} (mL)	d_{DLS} (nm)	$t_{sedim\text{-}theo}$ (h)	$t_{sedim\text{-}exp}$ (h)	$d_{Stokes\text{-}calc}$ (nm)
75	178	628	888	156
65	230	408	493	210
60	259	322	382	238
50	284	270	336	254
45	302	237	295	271
40	309	226	214	318

Photonic crystal formation relies on the self-assembly of monodispersed nanoparticles that can be achieved by using proper solvents and by controlling the surface tension and the evaporation rate. The surface tension of the utilized solvent serves as the primary driving force behind the self-assembly process, exerting a force that propels particles to minimize the distance between them. The surface tension of water is higher than that of ethanol; however, the evaporation rate of water is considerably slower. When two silica suspensions, one in water and one in ethanol, are drop casted on a substrate, the one in water will give a higher quality PC than the one in ethanol.

However, during EPD, surface tension is no longer the sole driving force. As mentioned previously, as long as the voltage is not too high, silica particles will create a fcc structure on the substrate surface. The rapid evaporation of the solvent during electrode recovery now plays a more significant role than the surface tension. The use of a solvent mixture can facilitate the self-assembly of the particles. Although, in general, water is not the most suitable solvent for EPD

because of its electrolysis and the generation of bubbles at the electrode surfaces. EPD was applied using different suspension solvents (alcohols and mixtures) with the following parameters: 25 V for 2 minutes. Only one batch was selected to do so, with a particle size between the extremes (SiO_2-65 ≈ 235 nm). The recovered electrodes showed disparate aspects depending on the solvent used (Figure 3). When ethanol was used as solvent, an uniform and flat film was obtained, but using 1-propanol or adding water to alcohol suspension leads to inhomogeneous films. Even if the amount of water used for the suspension solvent is low, it gave the worst results in terms of aspect. The zeta potential of every suspension was evaluated to give a better understanding of the EPD feasibility. Results gathered in Table 3 show a negative zeta potential for every suspension as expected for silica and in agreement with the anodic deposition. The value of ethanol is slightly higher in terms of potential, but above all, the standard deviation in ethanol is much lower indicating a more homogeneous suspension. Since ethanol produced smoother films compared to other solvents, we decided to favor its use rather than optimizing EPD parameters with 1-propanol or alcohol-water mixtures.

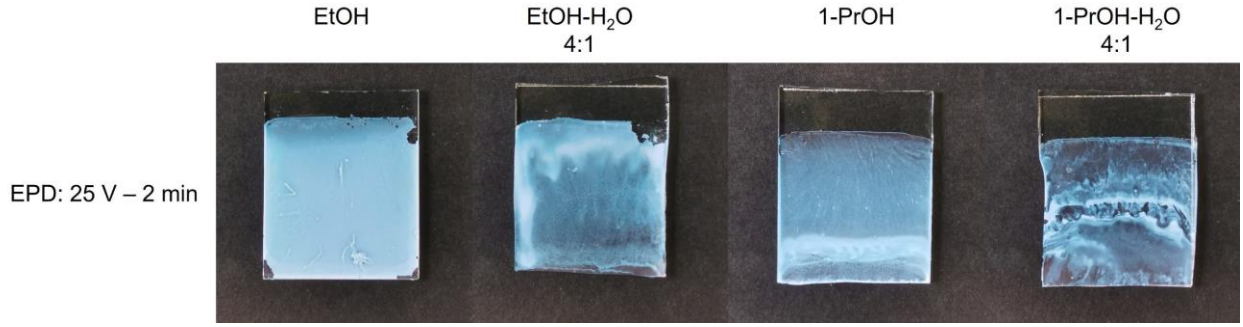

Figure 3. Optical photographs of films prepared by EPD from alcohol-based suspensions.

Table 3. Zeta potential of the different alcohol-water mixtures suspensions.

SiO_2-65	Zeta potential (mV)	Standard deviation
EtOH	-47.6	10.4

EtOH-H_2O (4:1)	-26.6	25.2
1-PrOH	-26.8	26.4
1-PrOH- H_2O (4:1)	-24.7	25.4

The disparate batches of silica particles were redispersed in ethanol (1 wt%) and deposited by EPD on ITO glass by applying a voltage of 25 V for a period of two minutes. Following the removal of the electrode from the suspension, the solvent was observed to evaporate in less than one minute, resulting in the formation of iridescent films. The films exhibited bright colors and a transparent aspect rather than the white and opaque appearance that would be anticipated for silica powder or aggregated films.

An XRD thin film pattern was recorded after EPD on a control sample (Figure 4). A single broad band was detected, with a maximum around 22°, confirming the amorphous state of silica. Indeed, this result is in agreement with the XRD patterns obtained for natural non-crystalline opal around the world.[28] Additionally, more distinct peaks were observed at 30.4°, 35.3°, 37.6° 50.6° and 60.3°, which were attributed to the Sn:In_2O_3 phase (Ia-3 space group (206)), corresponding to the conductive substrate.

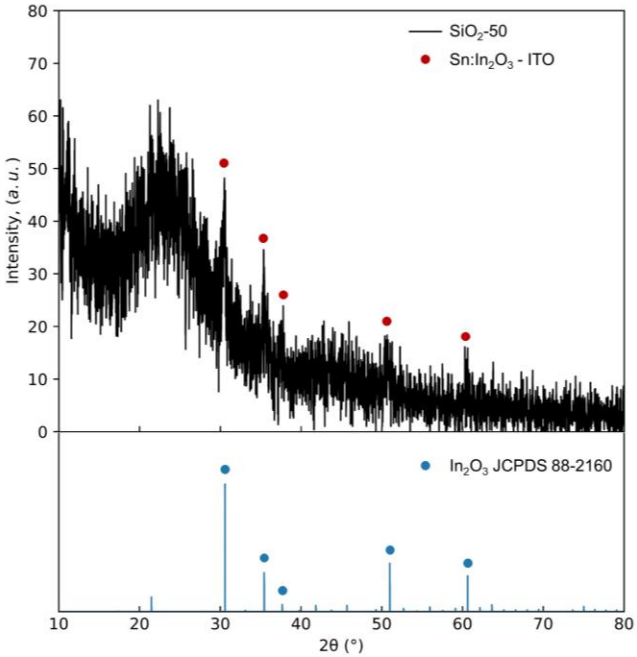

Figure 4. The XRD pattern of an average PCs films prepared by EPD from ethanol and SiO_2-50 particle suspension. In_2O_3 phase (JCPDS 88-2160) is also represented as a reference.

Self-assembly of nanoparticles leads to an opal structure that is responsible for the observed colors, in agreement with the Bragg-Snell equation (Equation 2):

$$\lambda_{max} = 2D_{(111)}\sqrt{(n_{eff}{}^2 - sin^2\theta)} \qquad \text{(Equation 2)}$$

Where, λ_{max} is the reflected wavelength for the first-order Bragg diffraction that corresponds to the partial band gap or stop band. The term "band gap" itself is preferred for 1D systems, while the terms "partial band gap" or "stop band" make more sense for 3D structure like opal structure where partial band gap can appear in only one direction. $D_{(111)}$ represents the lattice spacing of the face-centered cubic (fcc) structure, n_{eff} the effective refractive index and θ the incident angle. In the case of an SiO_2 opal structure with air between the nanoparticles, we can simplify the Equation 2 with the following parameters (Equation 3 & Equation 4):

$$D_{(111)} = \sqrt{\frac{2}{3}}d \qquad \text{(Equation 3)}$$

$$n_{eff} = \sqrt{f{n_1}^2 + (1-f){n_2}^2} \qquad \text{(Equation 4)}$$

With d the diameter of the silica nanoparticles, f = 0.74 the volume percentage of the fcc structure occupied by the silica nanoparticles, $n_1 = 1.45$ the refractive index of silica and $n_2 = 1$ the refractive index of air. For our study, it is possible to rewrite the first equation into a simplified one (Equation 5):

$$\lambda_{\max} = 1.633 d\sqrt{(1.33^2 - sin^2\theta)} \qquad \text{(Equation 5)}$$

Reflectance spectra with θ = 5° were measured, the λ_{max} and calculated $D_{(111)}$ were reported in Table 1 thanks to the Equation 5. A comparison of the diameters of the silica particles measured by DLS and calculated from reflectance spectra reveals a high degree of similarity, with differences of no more than 10 nm, which is within the range of the error bar measurement. Furthermore, thin film samples showed an angle-dependent structural color confirming the behavior of photonic crystal rather than photonic glass. Reflectance measurements were done from 5 to 45° on one sample, in order to extract the λ_{max} and to evaluate the associated particle diameter over angle range through the Equation 5 (Figure 5). The value of λ_{max} is decreasing when θ is increasing, from 627 to 539 nm, while the value of the diameter is fixed at 290 nm ± 2 nm, except for θ = 45° where the value of D is estimated at 294 nm. In general, all the thin films prepared by EPD exhibit angle-dependent structural coloration as illustrated in Figure 6. As the value of θ increased, a discernable minimum emerged at approximately 690 nm. This phenomenon is not intrinsic to the sample itself, but rather associated with to the substrate (ITO-glass).

In contrast with the findings of the preceding study conducted by Topçu *et al.*,[22] our washing and redispersing procedures did not result in the formation of photonic glass or pseudo-aggregates of silica particles. In their study, Topçu *et al.* emphasize that the drop casting of the as-synthesized silica colloids allows the production of photonic crystal whereas the drop casting of a redispersed

silica particles after washing and centrifugation steps leads to photonic glass. Despite the washing and centrifugation steps, only photonic crystals were formed, exhibiting angle-depend structural color. This discrepancy can be attributed to a prolonged redispersion period, an enhanced redispersion (by sonication), or the utilization of diminished power during the centrifugation step.

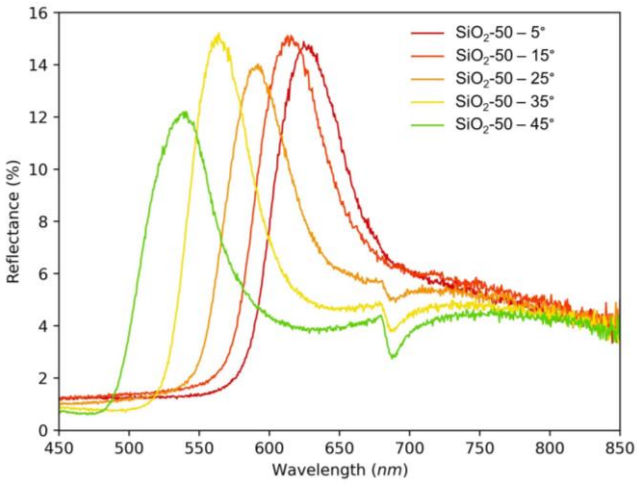

Figure 5. Reflection spectra of EPD PCs fabricated from an ethanol suspension containing 1 wt% of SiO_2-50 particles, at various angles.

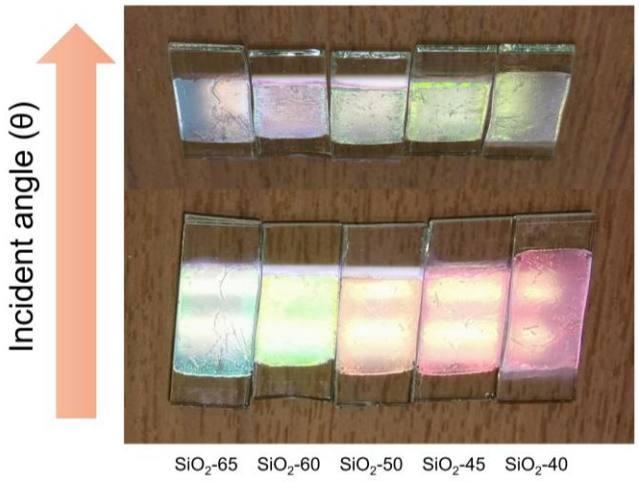

Figure 6. Optical photographs of films prepared by EPD at two different angles (≈ 5° and ≈ 60°).

In order to gain a more comprehensive understanding of the self-assembly of silica particles, we conducted surface and cross-section observations of PCs using SEM. The mean diameters and

standard deviations were calculated with the image processing and analysis software ImageJ (Table 1). Images revealed a close-packed fcc structure with few defects (Figure 7), which were predominantly associated with the lack of monodispersity in the nanoparticle batches. The fcc structure was emphasized by performing a Fast Fourier Transform (FFT), which converts a space domain into a frequency one. Because silica particles are ordered, the results of the FFT lead to organized bright spots forming a hexagonal surface symmetry. The extracted particle diameter values are slightly smaller than those measured by DLS or reflectance (approximately 10 nm), but still within the error range of the measurement. However, the values are always consistently smaller and may be attributed to a minor shift that could be a consequence of the threshold value utilized during the analysis conducted on ImageJ. Because the nanoparticles are well packed, the background of the picture might be overestimated to get SiO_2 particles with a define area, not overlapping or linked to each other. The cross-section images demonstrate the presence of opal structures with a thickness in a range of 2.5 to 5 μm (Figure S4) depending on the SiO_2 particles size. The number of layers ranged from 10 to 30, with a correlation to the particles size.

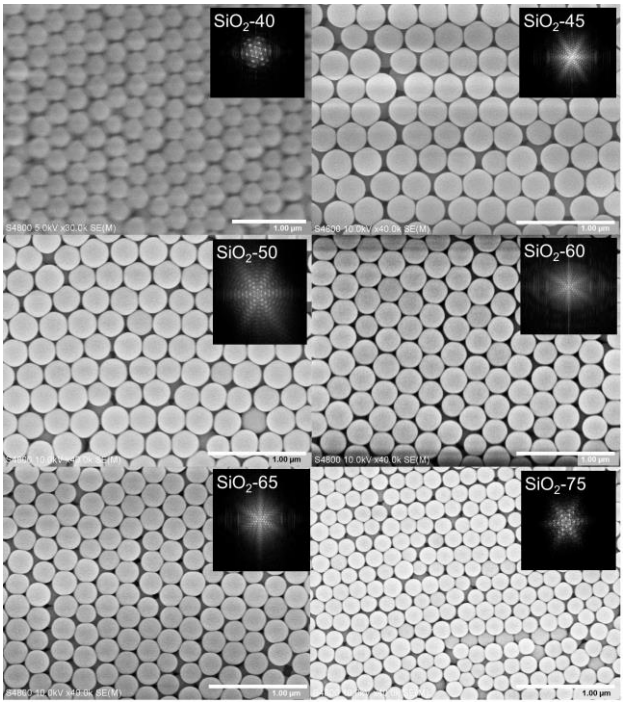

Figure 7. SEM images and associated FFT (inset) of EPD PCs fabricated from an ethanol suspension containing 1 wt% of SiO_2 particles. Scale bars have been redrawn for greater readability.

Moreover, the EPD technique is highly versatile, enabling control of the thickness through modification of the voltage and deposition time values. Depositions were conducted at 15 V (30 and 120 s) and at 25 V (30 and 120 s) on 2.5 × 1 cm rectangles ITO glass substrates. The associated cross section SEM pictures are presented in the Supporting Information (Figure S5). It can be noticed that for the lower voltage and time deposition (15 V – 30 s), only one layer of silica particles is deposited. By increasing the deposition time or the voltage (15 V – 120 s or 25 V – 30 s), the thickness was increased to 7-8 layers (1.75 µm) or 4 layers respectively (0.85 µm). The deposition at 25 V – 120 seconds gave the thicker film, around 27 layers (6.50 µm) in agreement with the previous results. EPD was also realized during 600 seconds (25 V) on similar substrates to prove the versatility of the technique (Figure S6, left). With those conditions, the film presents

a lower structural arrangement that can come from a lose of conductivity over the stacked layers and a weaker driving force overall. The thickness was evaluated at 17.7 µm, which represents approximately 70 layers. However, using larger substrates (5 × 2.5 cm rectangles) did not affect the structural arrangement for a deposition at 25 V – 120 seconds (Figure S6, right). The resulting thickness (5.60 µm, 24 layers) is slightly lower to the one for a smaller substrate (2.5 × 1 cm rectangles) and can be associated to a smaller voltage per surface unit. The measured thicknesses were gathered in the Table 4.

Table 4. EPD parameters applied and thickness of the formed films.

Substrate size (cm)	Applied voltage (V)	Deposition time (s)	Thickness (µm)	Number of layers
2.5 × 1	15	30	0.287	1
2.5 × 1	15	120	1.75	7-8
2.5 × 1	25	30	0.85	4
2.5 × 1	25	120	6.50	27
2.5 × 1	25	600	17.7	≈ 70
5 × 2.5	25	120	5.60	24

CONCLUSION

The work presented herein displays a fast and efficient way to get PCs starting from the synthesis of SiO_2 particles with tunable diameter, their dispersion in ethanol and their fast electrophoretic deposition in no more than two minutes. DLS, UV-Vis and SEM results agreed on homogeneous syntheses of nanoparticles where the volume of ethanol was varying while keeping the other parameters (volume, temperature, time) fixed. Artificial opal PCs showed bright colors, from blue

to red with an angle-dependent color thanks to their close-packed fcc structure, at short and long range. One could envision achieving optimized PC quality and reduce the defects by more effectively controlling the polydispersity of silica nanoparticles during the synthesis or by selecting precisely sized particles after synthesis.[29] However, the aim of this work was to promote a low-cost and efficient way to form PCs in a very short time, with a scalable technique. The specified partial band gap can be tuned over the whole visible spectrum by adjusting the nanoparticles size regarding the application or the photoactive compound it can be associated with.[30]

ASSOCIATED CONTENT

Supporting Information. Stöber method, sedimentation setup, graph of sedimentation rate of the whole series, SEM images of the cross-section. File: SupportingInformation.pdf

AUTHOR INFORMATION

Author Contributions

The manuscript was written through contributions of all authors. All authors have given approval to the final version of the manuscript.

ACKNOWLEDGMENT

C.L. acknowledges the financial support of NIMS and the France-Japan International Research Laboratory LINK (IRL3629, ANR-22-CE09-0015). The authors are very grateful to Lucile Vaschalde and Florent Baudouin (CNRS-Saint Gobain-NIMS, IRL 3629, Laboratory for Innovative Key Materials and Structures (LINK), National Institute for Materials Science (NIMS)).

ABBREVIATIONS

PCs, photonic crystals; EPD, electrophoretic deposition; TEOS, tetraethyl orthosilicate; ITO, indium tin oxide; RPM, rotation per minute; DLS, dynamic light scattering; FFT, fast Fourier transform.

REFERENCES

(1) Shu, Z.; Sun, X.; Xu, X.; Qin, M.; Li, J. Colloidal Photonic Crystals towards Biological Applications. *J. Mater. Chem. B* **2024**, *12* (35), 8488–8504.
(2) Sun, N.; Liu, X.; Liu, Y.; Zhao, R.; Xu, Z.; Li, S.; Lian, J.; Jiang, Q.; Wang, G. Enhancing the Brightness and Saturation of Noniridescent Structural Colors by Optimizing the Grain Size. *Nanoscale Adv.* **2020**, *2* (10), 4581–4590.
(3) Yu, S.; Ma, D.; Qi, C.; Yang, D.; Huang, S. All-In-One Photonic Crystals With Multi-Stimuli-Chromic, Color-Recordable, Self-Healable, and Adhesive Functions. *Adv Funct Materials* **2024**, 2411670.
(4) Hu, Y.; Tian, Z.; Ma, D.; Qi, C.; Yang, D.; Huang, S. Smart Colloidal Photonic Crystal Sensors. *Advances in Colloid and Interface Science* **2024**, *324*, 103089.
(5) Armstrong, E.; O'Dwyer, C. Artificial Opal Photonic Crystals and Inverse Opal Structures – Fundamentals and Applications from Optics to Energy Storage. *J. Mater. Chem. C* **2015**, *3* (24), 6109–6143.
(6) Mayoral, R.; Requena, J.; Moya, J. S.; López, C.; Cintas, A.; Miguez, H.; Meseguer, F.; Vázquez, L.; Holgado, M.; Blanco, Á. 3D Long-range Ordering in Ein SiO_2 Submicrometer-sphere Sintered Superstructure. *Advanced Materials* **1997**, *9* (3), 257–260.
(7) Jiang, P.; Bertone, J. F.; Hwang, K. S.; Colvin, V. L. Single-Crystal Colloidal Multilayers of Controlled Thickness. *Chem. Mater.* **1999**, *11* (8), 2132–2140.
(8) Xie, C.; Fan, T.; Wang, A.; Chen, S.-L. Enhanced Visible-Light Photocatalytic Activity of a TiO_2 Membrane-Assisted with N-Doped Carbon Quantum Dots and SiO_2 Opal Photonic Crystal. *Ind. Eng. Chem. Res.* **2019**, *58* (1), 120–127.
(9) Reculusa, S.; Ravaine, S. Synthesis of Colloidal Crystals of Controllable Thickness through the Langmuir−Blodgett Technique. *Chem. Mater.* **2003**, *15* (2), 598–605.
(10) Ran, X.; Ren, J.; Zhang, S.; Wu, Y.; Wu, S. Multicolor Electrochromic Display and Patterned Device Based on Hollow-SiO_2 -Supported WO_3 Photonic Crystals. *ACS Appl. Mater. Interfaces* **2023**, *15* (35), 41763–41771.
(11) Wu, Y.; Wang, X.; Zhong, W.; Zhang, S. Enhanced Visible Light Absorption of Bi2WO6/SiO2 with Abundant Adsorbed Oxygen for the Degradation of Organic Pollutant. *Particuology* **2024**, *88*, 210–217.
(12) Bayat, F.; Farshi, Z. S.; Arab Jafari, M. S.; Sharifi, M.; Chaghamirzaei, P.; Amani-Ghadim, A. R.; Jamshidi-Ghaleh, K. Colloidal Lithography: Synthesis and Characterization of SiO2 and TiO2 Micro-Bowel Arrays. *Materials Chemistry and Physics* **2025**, *332*, 130206.
(13) Uchikoshi, T. Colloidal Formation Process Based on Electrophoretic Phenomena of Charged Particles in Liquid Media and Electrode Reactions. *J. Ceram. Soc. Japan* **2024**, *132* (7), 387–396.
(14) Hassam, C. L.; Sciortino, F.; Nguyen, N. T. K.; Srinivasan, B.; Ariga, K.; Gascoin, F.; Grasset, F.; Mori, T.; Uchikoshi, T.; Thimont, Y.; Berthebaud, D. Robust, Transparent

Hybrid Thin Films of Phase-Change Material Sb_2S_3 Prepared by Electrophoretic Deposition. *ACS Appl. Energy Mater.* **2021**, *4* (9), 9891–9901.
(15) Nguyen, N. T. K.; Lebastard, C.; Wilmet, M.; Dumait, N.; Renaud, A.; Cordier, S.; Ohashi, N.; Uchikoshi, T.; Grasset, F. A Review on Functional Nanoarchitectonics Nanocomposites Based on Octahedral Metal Atom Clusters (Nb_6, Mo_6, Ta_6, W_6, Re_6): Inorganic 0D and 2D Powders and Films. *Science and Technology of Advanced Materials* **2022**, *23* (1), 547–578.
(16) Holgado, M.; García-Santamaría, F.; Blanco, A.; Ibisate, M.; Cintas, A.; Míguez, H.; Serna, C. J.; Molpeceres, C.; Requena, J.; Mifsud, A.; Meseguer, F.; López, C. Electrophoretic Deposition To Control Artificial Opal Growth. *Langmuir* **1999**, *15* (14), 4701–4704.
(17) Rogach, A. L.; Kotov, N. A.; Koktysh, D. S.; Ostrander, J. W.; Ragoisha, G. A. Electrophoretic Deposition of Latex-Based 3D Colloidal Photonic Crystals: A Technique for Rapid Production of High-Quality Opals. *Chem. Mater.* **2000**, *12* (9), 2721–2726.
(18) Tran, G. T. H.; Koike, M.; Uchikoshi, T.; Fudouzi, H. Fabrication of Polystyrene Colloidal Crystal Film by Electrophoretic Deposition. *Advanced Powder Technology* **2020**, *31* (8), 3085–3092.
(19) Katagiri, K.; Tanaka, Y.; Uemura, K.; Inumaru, K.; Seki, T.; Takeoka, Y. Structural Color Coating Films Composed of an Amorphous Array of Colloidal Particles via Electrophoretic Deposition. *NPG Asia Mater* **2017**, *9* (3), e355–e355.
(20) Takeoka, Y.; Yoshioka, S.; Takano, A.; Arai, S.; Nueangnoraj, K.; Nishihara, H.; Teshima, M.; Ohtsuka, Y.; Seki, T. Production of Colored Pigments with Amorphous Arrays of Black and White Colloidal Particles.
(21) Muldarisnur, M.; Marlow, F. Structure and Optical Properties of Opal Films Made by an Out-of-Plane Electric Field-Assisted Capillary Deposition Method. *ACS Omega* **2022**, *7* (9), 8084–8090.
(22) Liesegang, M.; Milke, R. Australian Sedimentary Opal-A and Its Associated Minerals: Implications for Natural Silica Sphere Formation. *American Mineralogist* **2014**, *99* (7), 1488–1499.
(23) Stöber, W.; Fink, A.; Bohn, E. Controlled Growth of Monodisperse Silica Spheres in the Micron Size Range. *Journal of Colloid and Interface Science* **1968**, *26* (1), 62–69.
(24) Tan, C. G.; Bowen, B. D.; Epstein, N. Production of Monodisperse Colloidal Silica Spheres: Effect of Temperature. *Journal of Colloid and Interface Science* **1987**, *118* (1), 290–293.
(25) Ghimire, P. P.; Jaroniec, M. Renaissance of Stöber Method for Synthesis of Colloidal Particles: New Developments and Opportunities. *Journal of Colloid and Interface Science* **2021**, *584*, 838–865.
(26) Gao, W.; Rigout, M.; Owens, H. Facile Control of Silica Nanoparticles Using a Novel Solvent Varying Method for the Fabrication of Artificial Opal Photonic Crystals. *J Nanopart Res* **2016**, *18* (12), 387.
(27) Topçu, G.; Güner, T.; Demir, M. M. Non-Iridescent Structural Colors from Uniform-Sized SiO_2 Colloids. *Photonics and Nanostructures - Fundamentals and Applications* **2018**, *29*, 22–29.
(28) Sodo, A.; Casanova Municchia, A.; Barucca, S.; Bellatreccia, F.; Della Ventura, G.; Butini, F.; Ricci, M. A. Raman, FT-IR and XRD Investigation of Natural Opals. *J Raman Spectroscopy* **2016**, *47* (12), 1444–1451.
(29) Ni, P.; Dong, P.; Cheng, B.; Li, X.; Zhang, D. Synthetic SiO_2 Opals. *Adv. Mater.* **2001**, *13* (6), 437–441.

(30) Dechézelles, J.-F.; Aubert, T.; Grasset, F.; Cordier, S.; Barthou, C.; Schwob, C.; Maître, A.; Vallée, R. A. L.; Cramail, H.; Ravaine, S. Fine Tuning of Emission through the Engineering of Colloidal Crystals. *Phys. Chem. Chem. Phys.* **2010**, *12* (38), 11993.

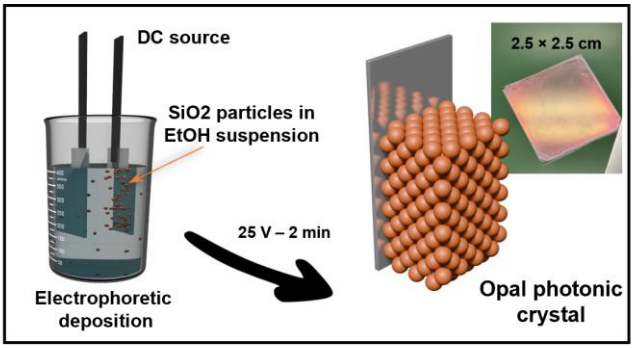
DC source
SiO2 particles in
EtOH suspension
25 V – 2 min
Electrophoretic
deposition
2.5 × 2.5 cm
Opal photonic
crystal

TOC Graphic